Global Change Biology (2003) **9,** 1005–1021

Major disturbance events in terrestrial ecosystems detected using global satellite data sets

CHRISTOPHER POTTER*, PANG-NING TAN†, MICHAEL STEINBACH†, STEVEN KLOOSTER‡, VIPIN KUMAR†, RANGA MYNENI§ and VANESSA GENOVESE‡
**NASA Ames Research Center, Moffett Field, CA, USA, †University of Minnesota, Minneapolis, MN, USA, ‡California State University Monterey Bay, Seaside, CA, USA, §Boston University, Boston, MA, USA*

Abstract

Ecosystem scientists have yet to develop a proven methodology to monitor and understand major disturbance events and their historical regimes at a global scale. This study was conducted to evaluate patterns in an 18-year record of global satellite observations of vegetation phenology from the Advanced Very High Resolution Radiometer (AVHRR) as a means to characterize major ecosystem disturbance events and regimes. The fraction absorbed of photosynthetically active radiation (FPAR) by vegetation canopies worldwide has been computed at a monthly time interval from 1982 to 1999 and gridded at a spatial resolution of 0.5° latitude/longitude. Potential disturbance events of large extent (> 0.5 Mha) were identified in the FPAR time series by locating anomalously low values (FPAR-LO) that lasted longer than 12 consecutive months at any 0.5° pixel. We find that nearly 400 Mha of the global land surface could be identified with at least one FPAR-LO event over the 18-year time series. The majority of these potential disturbance events occurred in tropical savanna and shrublands or in boreal forest ecosystem classes. Verification of potential disturbance events from our FPAR-LO analysis was carried out using documented records of the timing of large-scale wildfires at locations throughout the world. Disturbance regimes were further characterized by association analysis with historical climate anomalies. Assuming accuracy of the FPAR satellite record to characterize major ecosystem disturbance events, we estimate that nearly 9 Pg of carbon could have been lost from the terrestrial biosphere to the atmosphere as a result of large-scale ecosystem disturbance over this 18-year time series.

Keywords: carbon, climate, disturbance, ecosystems, remote sensing

Received 13 September 2002; revised version received 12 February 2003 and accepted 17 February 2003

Introduction

An ecological disturbance is an event that results in a sustained disruption of ecosystem structure and function (Pickett & White, 1985; Tilman, 1985), generally with effects that last for time periods longer than a single seasonal growing cycle for native vegetation. Physical disturbance categories include fires, hurricanes, floods, droughts, lava flows, and ice storms. Biogenic disturbance categories include the impacts of herbivorous insects, mammals, and pathogens. Anthropogenic disturbance categories include logging, deforestation, drainage of wetlands, clearing for cultivation, chemical pollution, and alien species introductions. Many of these events alter ecosystem productivity and resource availability (light and nutrient availability) for organisms on large spatial and temporal scales.

Ecosystem disturbances can also contribute to the current rise of carbon dioxide (CO_2) levels in the atmosphere (Potter, 1999; Schimel *et al*., 2001). Because major 'pulses' of CO_2 from terrestrial biomass loss can be emitted to the zatmosphere during large disturbance events, the timing, location, and magnitude of vegetation disturbance is presently a major uncertainty in understanding global carbon cycles (Canadell *et al*., 2000). Elevated biogenic sources of CO_2 have global implications for climatic

Correspondence: Christopher Potter, NASA Ames Research Center, Moffett Field, CA, USA, tel. +650 604 6164, fax +650 604 4680, e-mail: cpotter@gaia.arc.nasa.gov

change, which can in turn affect a vast number of species on Earth and the functioning of virtually all ecosystems.

Despite the importance of ecosystem disturbance for improved understanding of terrestrial carbon exchange with the atmosphere, there is no verified method to document major CO_2 emission events resulting from disturbances of all types on a global basis over time periods of at least a decade. Numerous studies have been conducted to quantify carbon emissions from single categories of disturbance, principally biomass burning events, and generally with national or continental levels of resolution. These studies include Kurz & Apps (1999), Houghton *et al*. (1999), Murphy *et al*. (2000), Amiro *et al*. (2001) for portions of North America, Fearnside (1997), Nepstad *et al*. (1999), Potter *et al*. (2001) for portions of South America, Scholes *et al*. (1996), Barbosa *et al*. (1999) for portions of Africa, Houghton & Hackler (1999) for portions of Southeast Asia, and Hurst *et al*. (1994) for Australia. Several studies have dealt with global level effects of deforestation of carbon emissions (Andreae, 1991; Houghton, 1999; Potter, 1999). However, we are aware of no study approaches to date that have been global in scope, covered more than a decade of analysis, and encompass all potential categories of major ecosystem disturbance – physical, biogenic, and anthropogenic – using an equivalent method of detection and analysis.

Leafy vegetation cover is likely the most fragile and therefore perhaps the single most vulnerable biotic component of terrestrial ecosystems to detectable alteration during disturbance events. Vegetation leaf cover burns relatively easily or can be readily blown down or cut to the ground. Leaf litter then decomposes rapidly to blend in with background soil attributes, at least compared to the large woody biomass components of shrub, woodland, and forest ecosystems.

Earth-observing satellites have monitored leafy vegetation cover on land, also called 'greenness' cover, for close to 20 years (Myneni *et al*., 1998). Like the Normalized Difference Vegetation Index (NDVI), a common measure of greenness cover is the fraction of photosynthetically active radiation, or FPAR (Knyazikhin *et al*., 1998), intercepted by vegetation canopies, ranging from zero (on barren land) to 100% (for dense cover). In theory, the higher the FPAR level observed over the course of a seasonal plant growing cycle, the denser the green leaf cover and (presumably, on average) the less disturbed the vegetation cover, and/or the longer the time period since the last major disturbance. It is plausible that any significant and sustained decline in vegetation FPAR observed from satellites represents a disturbance event, a hypothesis, which is, however, subject to verification from independent records of such disturbance events.

Consequently, the question we pose in this study is whether a multiyear time series of historical satellite FPAR can be used to detect most large-scale vegetation disturbance events on the global land surface? We present a method designed to detect major disturbance events using satellite FPAR data sets comprised of 18 continuous years of monthly observations. The geographical distributions and temporal variations in these potential disturbance events are characterized. Records of major wildfires worldwide since 1982 are used to verify the accuracy of our disturbance detection methods. Finally, we characterize associations of potential disturbance events with climate events, such as major droughts, and discuss implications for potential CO_2 losses (to the atmosphere) from major disturbance events leading to destruction of terrestrial biomass globally.

Methods to detect and understand major disturbance regimes

In analysis of a multiyear time series of vegetation dynamics from satellites, it should be possible to move beyond single disturbance events to conduct studies of 'disturbance regimes'. A disturbance regime is defined according to the spatial, temporal, and qualitative nature of disturbance events occurring within any given ecosystem type (Heinselman, 1973). A natural disturbance regime (such as a forest fire cycle) can be described in terms of spatial extent (hectares) and distribution (patchiness), as well as the frequency and seasonality of its occurrence over time, and its severity or intensity (i.e. the energy released per unit area and time). We describe below approaches to better understand major ecosystem disturbance regimes on a global level using a 18-year record of monthly satellite-observed FPAR.

Monthly FPAR values for the land surface were computed from the Advanced Very High Resolution Radiometer (AVHRR) data sets covering the period 1982–1999. This FPAR data set was generated using canopy radiative transfer algorithms (Knyazikhin *et al*., 1998), which are designed to generate improved vegetation products for input to terrestrial carbon flux calculations. These radiative transfer algorithms, developed for the MODIS (MODerate resolution Imaging Spectroradiometer) aboard the NASA Terra satellite platform, account for attenuation of direct and diffuse incident radiation by solving a three-dimensional formulation of the radiative transfer process in vegetation canopies. Monthly composite data from channels 1 (visible) and 2 (near-infrared) of the AVHRR have been processed according to the MODIS radiative transfer algorithms and aggregated over the global land surface to 0.5° latitude/longitude resolution. This aggregation level generates single grid cell (pixel) areas ranging between 0.1 Mha at 70°N latitude to 0.3 Mha at the equator per 0.5° resolution pixel ($1\,\text{Mha} = 10^6\,\text{ha} = 10^4\,\text{km}^2$).

The observed FPAR time series at each pixel was first detrended (see example in Fig. 1a) using a linear adjustment, which is necessary to minimize the possibility that, in cases where there is a gradual but marked increase in monthly FPAR over the 18-year time series (Fig. 1b), any potential disturbance events occurring relatively near the end of the series are not overlooked. Because of the dominant seasonal oscillations in vegetation phenology observed throughout the globe, our detrended FPAR time series was subsequently 'deseasonalized' by computing the 12-month running average time series for every 0.5° pixel location.

An algorithm was next developed to identify any significant and sustained declines in FPAR during the 18-year time series. We hypothesize that significant declines in average annual FPAR levels can be defined according to greater than 1.7 standard deviations (SD) below (LO) the 18-year average FPAR computed for any specific pixel location (Fig. 1). A 'sustained' disturbance event would be defined as any decline in average annual FPAR levels (at an assigned significance level) that lasts for a temporal threshold value of at least 12 consecutive monthly time steps at any specific pixel location. The logic used here is that an actual disturbance involves a sustained decline in FPAR because the structure of the vegetation cover has been severely altered or destroyed during the disturbance event, to a magnitude that lowers FPAR significantly for at least one seasonal growing cycle, after which time regrowth and recovery of the former vegetation structure may permit FPAR to increase again.

It is assumed that fairly common effects of atmospheric interference with the AVHRR channel signals, such as heavy cloud cover or smoke-derived aerosols, would not persist (e.g. as a false disturbance event) in the multi-year time series and thereby generate a FPAR-LO pattern longer than about 6 months. By design, our disturbance algorithm should be insensitive to heavy cloud cover or smoke effects that occur practically every year during the same season, or only episodically for 1 or 2 months at a time. If an interference effect occurs every year at about the same time, it will be eliminated automatically as part of the deseasonalization algorithm. One possible exception to this principle could be persistent atmospheric interference effects generated by major volcanic eruptions, such as the Pinatubo event of late 1991.

While, it may be the case that FPAR can vary from year-to-year during dormant (nongrowing) seasons, it is also possible for actual disturbances to occur during the dormant season, such as ice damage or an extremely low snow season. Therefore, we cannot justify excluding the dormant season from our time series analysis. Furthermore, periodic errors in leafless canopy (vs full canopy) estimates of FPAR are not likely to have a major impact on the long-term (18 year) 12-month running mean FPAR, against which we have detected any and all of the FPAR-LO events.

In the use of a one-sided (LO) statistical *t*-test, rejection of the null hypothesis means that there is no difference between the 18-year average for the monthly FPAR level and the consistent FPAR-LO level identified in a string of ≥ 12 consecutive time steps. A SD ≥ 1.7 represents the 95% LO confidence level, a SD ≥ 2.0 represents the 97% LO confidence level, and a SD ≥ 2.6 represents the 99% LO confidence level (Stockburger, 1998). Since we have first detrended the FPAR time series by linear regression, the resulting data series should more closely approximate a normal distribution. The resulting data series have 17 degrees of freedom for tests of significance (18 years $-$ 1 for a one-tailed test).

The statistical confidence level for FPAR-LO may serve as a useful index of disturbance intensity, possibly in combination with the maximum consecutive months observed in a time series of FPAR-LO. To complete the characterization of a disturbance regime within any given ecosystem type, the global FPAR images can be used to estimate the spatial extent of contiguous 0.5° resolution pixels showing similar levels of FPAR-LO disturbance intensity (as defined above), together with any repeated sequences of sustained FPAR-LO events within the multi-year time series, and the time of the year when a sustained FPAR-LO event typically occurs.

Results from global FPAR time series

We have applied the methods described above to the 18-year FPAR time series from global AVHRR data at 0.5° resolution to identify potential disturbance events in terrestrial ecosystems. Beginning with SD ≥ 1.7 (95% confidence) for the level of disturbance intensity, we can detect 1856 pixel locations at the threshold of 12 consecutive monthly time steps for FPAR-LO events (Fig. 2a, b). Summed over 18-year, these pixels together cover a total area of 398 Mha, which represent about 3% of the 14 250 Mha nonbarren (nonice and nondesert) global land surface (DeFries & Townshend, 1994).

At SD ≥ 2.0 (97% confidence) for the level of disturbance intensity, we detect far fewer (i.e. 269 pixel locations) at the threshold of > 12 consecutive monthly time steps for FPAR-LO events that together cover a total area of 60 Mha. Of these, we detect no pixel locations at SD ≥ 2.6 (99% confidence) for the level of disturbance intensity lasting > 12 consecutive months of FPAR-LO events. Consequently, we define two levels of potential disturbance intensity, and unless otherwise mentioned, the subsequent analysis presented in this section is based on all potential disturbance events detected a SD ≥ 1.7 level for the threshold of > 12 consecutive monthly time steps for

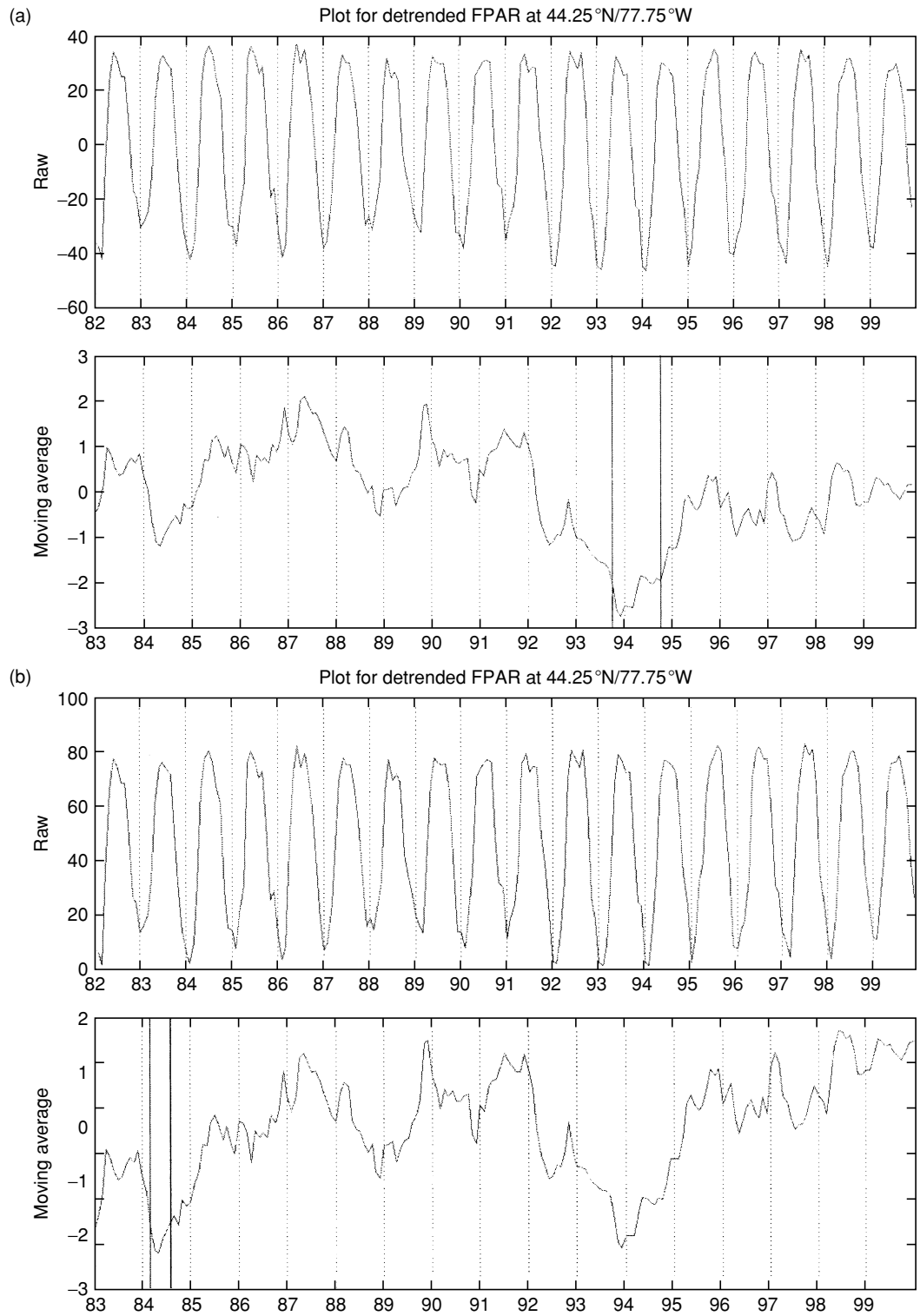

Fig. 1 (a) Example of detrended FPAR raw values and Z-score line plots for an FPAR-LO lasting > 12 consecutive months. Location is a temperate forest ecosystem in southern Ontario. The FPAR-LO event begins in 1993 and lasts for 14 consecutive months. (b) Original FPAR (before detrending), showing the loss of sensitivity to detection of the 1993 FPAR-LO event. Vertical lines show the longest consecutive period of anomalously LO monthly values.

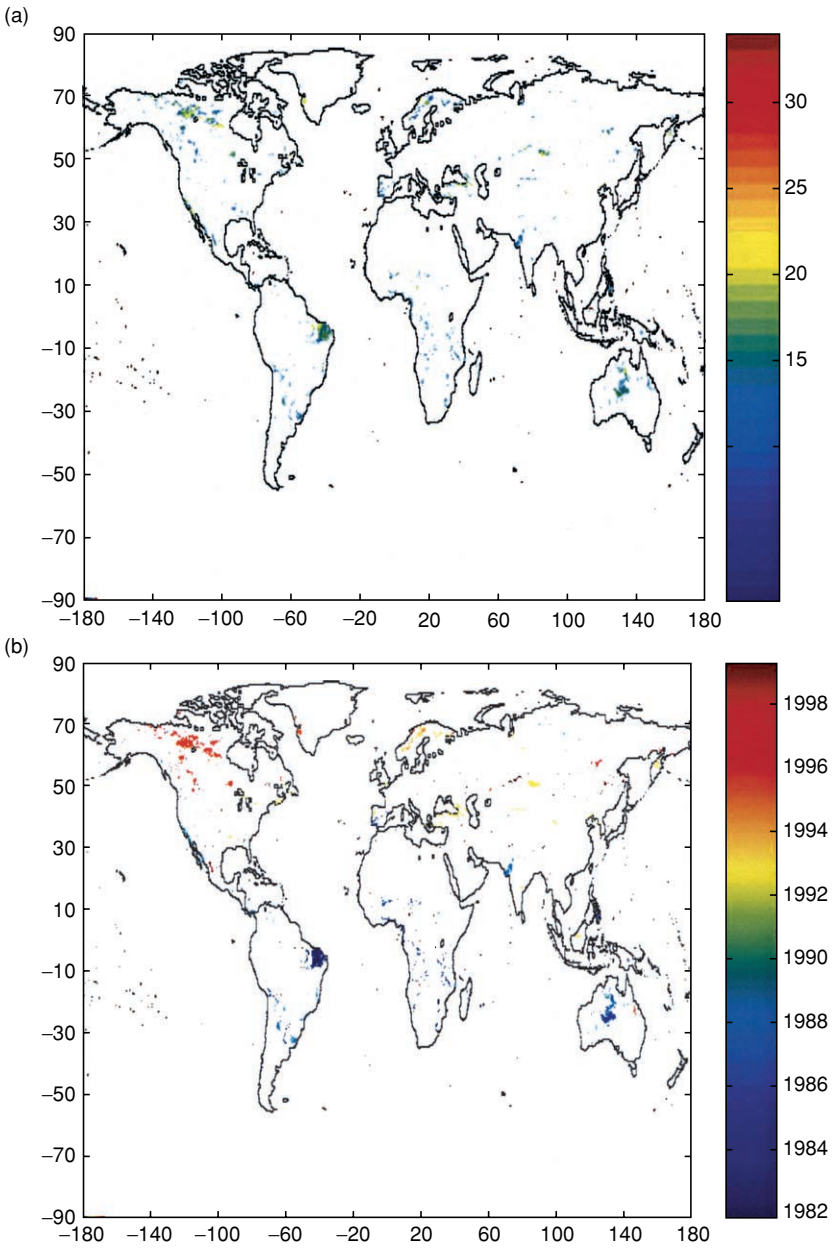

Fig. 2 Global maps of potential major disturbance events identified in the 18-year AVHRR time series. (a) Number of consecutive months lasting >12 months at SD ≥1.7 for FPAR-LO. (b) First month and year for SD ≥1.7 FPAR-LO lasting >12 consecutive months.

FPAR-LO events, which is the largest set of statistically significant pixel locations available to us for analysis.

Geographic distribution patterns

The distribution with latitude of all pixel areas detected at a SD ≥1.7 level lasting >12 consecutive months of FPAR-LO shows two major zones of equal concentration (Fig. 3a), with 35% of the total area located in the zone from 40° to 70°N, and 36% of the total area located in the zone from 5° to 35°S. With SD ≥ 2.0 as the level of disturbance intensity, areas with >12 consecutive months for FPAR-LO were detected mainly (34%) in the zone from 1° to 10°S. The distribution among major global vegetation classes (delineated for this study according to DeFries & Townshend, 1994) of pixel areas from FPAR-LO events (Fig. 2a) at SD ≥1.7 (and also at SD ≥2.0) shows that about 50% of the potentially disturbed area were located in savanna, grasslands, and shrublands (Table 1), whereas nearly 20% of area were located in evergreen needleleaf and tundra/boreal forests and another 10% in grasslands.

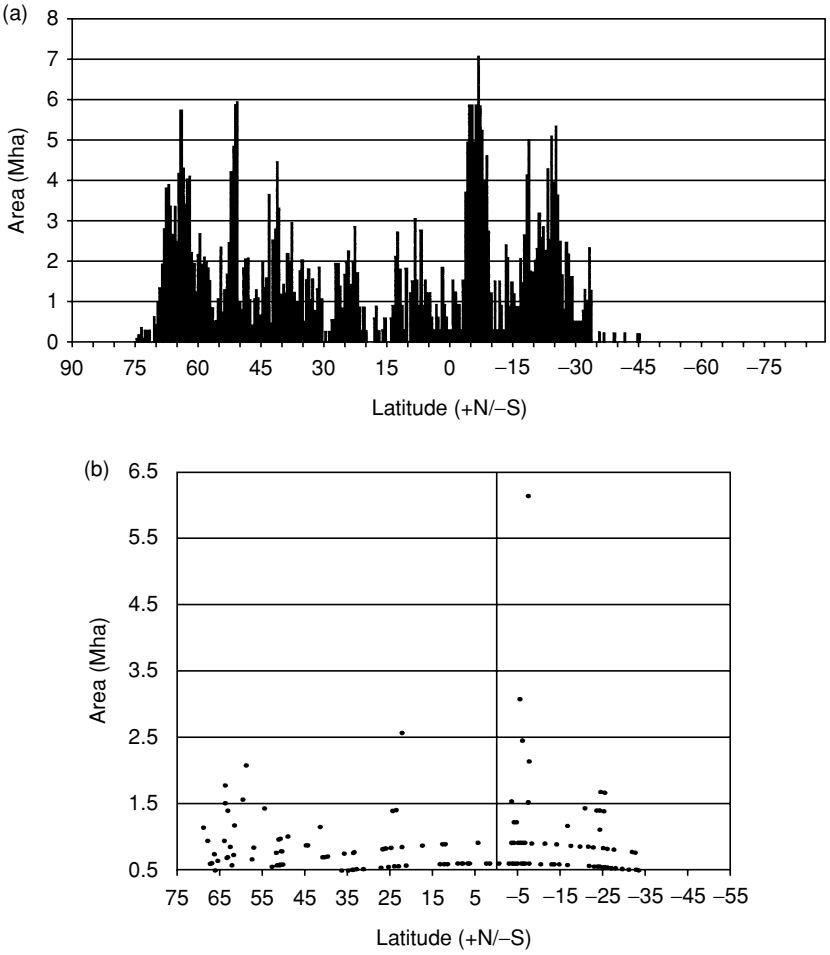

Fig. 3 Distribution according to latitude of pixel areas detected at a SD ≥ 1.7 level lasting > 12 consecutive months of FPAR-LO. (a) All pixel areas. (b) Contiguous pixel areas > 0.5 Mha potential disturbance area.

Table 1 Area of FPAR-LO events detected over 18-year AHVRR time by global vegetation class (DeFries & Townshend, 1994)

Vegetation class	Area (Mha)	Percent	Area (Mha)	Percent
Evergreen needleleaf forests	23.1	5.8	1.2	2.1
Evergreen broadleaf forests	71.7	18.2	11.1	18.7
Deciduous needleleaf forests	10.5	2.6	0.4	0.8
Deciduous broadleaf forests	15.6	4.0	1.4	2.4
Mixed forests	12.4	3.1	2.0	3.3
Savanna woodlands	99.7	25.2	21.5	36.2
Wooded grasslands	62.0	15.7	8.1	13.6
Closed shrublands	0.8	0.2	0.0	0.0
Grasslands	40.9	10.4	6.2	10.4
Croplands	13.0	3.3	2.2	3.6
Desert	1.1	0.3	0.3	0.5
Tundra/boreal forest	44.4	11.2	5.1	8.5
Total	395.1	100.0	59.6	100.0

The distribution of contiguous 0.5° pixel areas for FPAR-LO events vs. latitude zone (Fig. 3b) implies that the potentially largest disturbance events in the 18-year time series have occurred mainly in the zones from 55° to 70°N and from 3° to 25°S. Contiguous areas were defined as two or more neighboring 0.5° pixel locations that share a common month and year for the initiation of a FPAR-LO event lasting > 12 consecutive months. The largest of these contiguous FPAR-LO areas, each at > 1.5 Mha of potential disturbance, were detected mainly in

savanna, grassland, and boreal forest vegetation classes (DeFries & Townshend, 1994). A total of six contiguous areas of >2 Mha in potential disturbance were identified in the data set, with four of these areas located in the northeastern portion of Brazil beginning 1983, including the single largest contiguous area of potential disturbance at 6.1 Mha (centered 7°S, 39°W). The other two contiguous areas of >2 Mha in potential disturbance were located in northwestern Canada (centered 59°N/122°W) during 1995 and in western India (centered 22°N/71°E) during 1986.

Temporal variations

When viewed in terms of the consecutive monthly time steps for FPAR-LO >12 months, the distribution of all pixel areas at SD ≥ 1.7 (Fig. 2a), shows that 91% of the potential disturbance area coverage had a duration of between 12 and 20 consecutive months for FPAR-LO events (Fig. 4). Beginning from the maximum concentration of pixel areas at 13 consecutive months FPAR-LO (33% of all pixels), the decline in area coverage with an increase in the number of consecutive monthly time steps was nearly exponential ($R^2 = 0.93$), out to the maximum value of 34 consecutive months of FPAR-LO. We could detect no significant trends in the relationship between latitude zone and number of consecutive monthly time steps for FPAR-LO events at SD ≥ 1.7. However, most of the relatively long events of between 20 and 25 consecutive months for FPAR-LO were detected in the boreal forest vegetation class (DeFries & Townshend, 1994) located in latitude zones between 40° and 70°N. These temporal patterns in potential disturbance events imply that FPAR recovers from disturbance relatively slowly in high latitude zones (>40°N). Nonetheless, some the longest potential disturbance events of >24 consecutive months for FPAR-LO were detected in the tropical evergreen forest vegetation class (DeFries & Townshend, 1994). With SD ≥ 2.0 for the level of disturbance intensity, we find that 100% of the potential disturbance area coverage had duration between 12 and 20 consecutive monthly time steps for FPAR-LO events, which might be expected if these potentially disturbed areas have recovered fairly rapidly from past disturbance of green leaf cover or woody biomass.

The distribution according to the start month for pixel areas detected at the SD ≥ 1.7 level of FPAR-LO lasting >12 consecutive months shows that the periods of highest detection frequency were in 1982–1983 and 1995–1996 (Fig. 5). The consecutive 12-month periods with the highest area detected as potentially disturbed were in 1983 when over 75 Mha yr^{-1} of potentially disturbed area was identified (out of the total of 398 Mha), followed by periods in 1996 when over 60 Mha yr^{-1} of potentially disturbed area was identified.

There is a significant linear trend ($R^2 = 0.56$, $P < 0.05$) between latitude zone and the year(s) for most frequent detection of the start of FPAR-LO events. Specifically, in the relatively low latitude zones between 5° and 45°S, the majority of FPAR-LO events lasting >12 consecutive months were detected as starting within the period from 1982 to 1987. In the relatively high latitude zones between 40° and 70°N, the majority of FPAR-LO events >12 consecutive months were detected as starting within the period from 1991 to 1999.

Our method detected only a single pixel location that had two FPAR-LO events (SD ≥ 1.7) occurring within this 18-year time series. This pixel was located in grasslands of northern Australia (centered 21°S and 133°E), where two FPAR-LO events lasting >12 consecutive months were detected within a single 3-year period beginning in 1985. There was a brief recovery of FPAR between these two LO events when several months of near-average rainfall was recorded within what was otherwise an extended three-year drought period (New *et al*., 2000), when precipitation generally remained 1.7 SD below the 18-year mean.

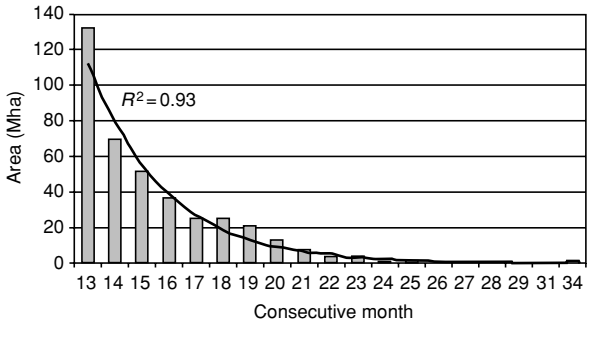

Fig. 4 Distribution according to consecutive monthly time steps of all pixel areas detected at a SD ≥ 1.7 level of FPAR-LO.

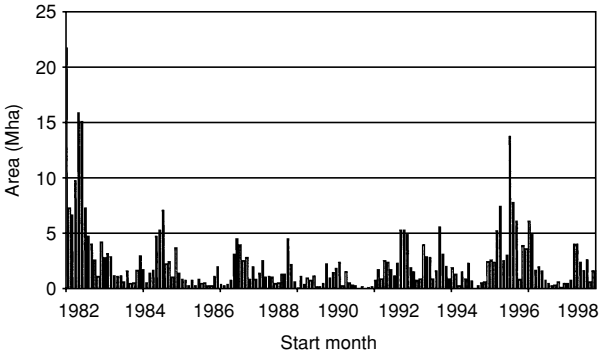

Fig. 5 Distribution according to start month of all pixel areas detected at a SD ≥ 1.7 level of FPAR-LO level lasting >12 consecutive months.

Verification using historical disturbance events

Having detected numerous sustained FPAR-LO events within the global 18-year AVHRR data set, verification of actual changes in ecosystem structure (i.e. large scale disturbances) should be based on the demonstration of close associations between the results shown in Fig. 2 and independently confirmed, well-documented historical disturbance events. For the purposes of this study, a large-scale disturbance event must be defined according to single cell areas at 0.5° pixel resolution, which range from 0.1 to 0.3 Mha, starting from the polar zones and moving to the equator. Consequently, we surmise that this global FPAR data set inherently limits the types of well-documented historical disturbances that can be used for algorithm verification, namely to potential events that exceed 0.5 Mha in affected land area. We note that although an area of 0.5 Mha could be comprised of several FPAR 0.5° pixels, depending on the latitude zone, less than 100% of these pixel areas is likely to be heavily vegetated and therefore subject to ecosystem disturbance patterns that our methods could detect. For this reason, we hypothesize that well-documented disturbance events should ideally exceed 0.5 Mha in area to be included in a verification data set for this study. Our analysis, therefore, excluded all small-scale (< 1 km) deforestation activities such as those documented in humid tropical forests (Kaufman *et al*., 1998).

The principal set of historical disturbance events available to us for algorithm verification are well-documented wildfires that burned areas reported to cover several Mha in a single year or vegetation growing season. A list of such events was compiled (Table 2) using publications and reports from the global fire literature (Biasutti & Marchetti, 1996; Goldammer & Furyaev, 1996; Swetnam, 1996; Kasischke *et al*., 1999). This list in Table 2 is not intended to represent an exhaustive set of major fire events over the 18-year period of the global FPAR record, but instead is a list of the largest fire events that could be confirmed for their timing of initiation (to within about 6 months) and geographical location (to within approximately 2° latitude and longitude). Additional references have been located for some of these fire events. Starting in the mid-1990s, several of these wildfires have been confirmed for timing and location using Landsat and other relatively high-resolution satellite images (Arino & Plummer, 1999).

We find that within each geographical area of the confirmed wildfire events listed in Table 2, our disturbance detection method confirms a FPAR-LO event at (or near) the SD ≥ 1.7 level lasting > 12 consecutive months and starting during the reported time period of actual fire activity. Time series plots of the original (raw) detrended FPAR values and the deseasonalized Z-score FPAR anomalies are shown (Fig. 6) for six selected wildfire events listed in Table 2. As an example, the FPAR time series for a representative location in East Kalimantan, Indonesia (Fig. 6a) shows a significant FPAR-LO event (SD ≥ 2.0) in 1983 and another notable event in 1997 that nearly reached the FPAR-LO level of SD ≥ 1.7. As shown in Fig. 6b, extensive woodland fires in the Ivory Coast of Africa 1982–1983 were readily detected at the FPAR-LO

Table 2 List of largest confirmed wildfires on record in the 1980s and 1990s

Year	Location	Area burned (Mha)	Latitude/longitude	References
1982 and 1983	East Kalimantan, Indonesia	5	0°N/117°E	(Hoffmann *et al*., 1999)
1982 and 1983	Ivory coast	12	7°N/5°W	
1987	Russia–China*	6–11	51°N/127–128°E	(Cahoon *et al*., 1991, 1994)
1988	Yellowstone Wyoming, USA	0.5	44.6°N/110.7°W	(Shovic, 1988; Jeffrey, 1989)
1989	Manitoba, Canada†	0.5	51°N/97°W	
1996 and 1997	Mongolia	11	46–50°N/100–110°E	
1997	Alaska, USA‡	0.2	63–64°N/159°W	(Boles & Verbyla, 2000)
1997	Kalimantan and Sumatra, Indonesia§	9	0–4°S/110–115°E 0–4°S/105°E	(Hoffmann *et al*., 1999)
1998	Mexico§	0.5	17–22°N/94–98°W	(Galindo *et al*., 2003)

Source: European space agency earth watching fires archive (Biasutt & Marchetti, 1996) [ftp://earth1.esrin.esa.it/pub/ew/fires/]. Canadian interagency fire center reports, Winnipeg, Manitoba.

*In Da Hinggan–Dzhagdy mountains coniferous forests; fire destroyed the town of Xilinji in Russia east of Lake Baikal between the Amur and Lena rivers.

†Fire started near Lake Manitoba and spread northward for 800 km.

‡Inowak fire (100 miles SW of McGrath, AK) plus the Simels and Magitchlie Creek fires in the Galena District.

§Fire location has been confirmed using Landsat and ATSR (Along Track Scanning Radiometer) satellite images (Arino & Plummer, 1999).

level of SD ≥ 2.0. Locations of the large forest fires of 1987 reported on the Russia–China boarder area of the Da Hinggan–Dzhagdy mountains shows a significant FPAR-LO event (SD ≥ 2.0) during this period of 1987 (Fig. 6c). Wildfires reported in Manitoba, Canada during 1989, in Mongolia during 1987 and 1996, and in Mexico during 1998 (Fig. 6d–f) were also verified as FPAR-LO events (SD ≥ 1.7).

For all but one of the disturbance events listed in Table 2, the presence of wildfires could be confirmed using an independent satellite smoke-aerosol index (SAI). An example of the SAI is shown for East Kalimantan, Indonesia in Fig. 7, along with monthly precipitation anomalies (New *et al*., 2000) for this same pixel location in Fig. 6a. Smoke from biomass burning produces UV-absorbing tropospheric aerosols, which can be measured

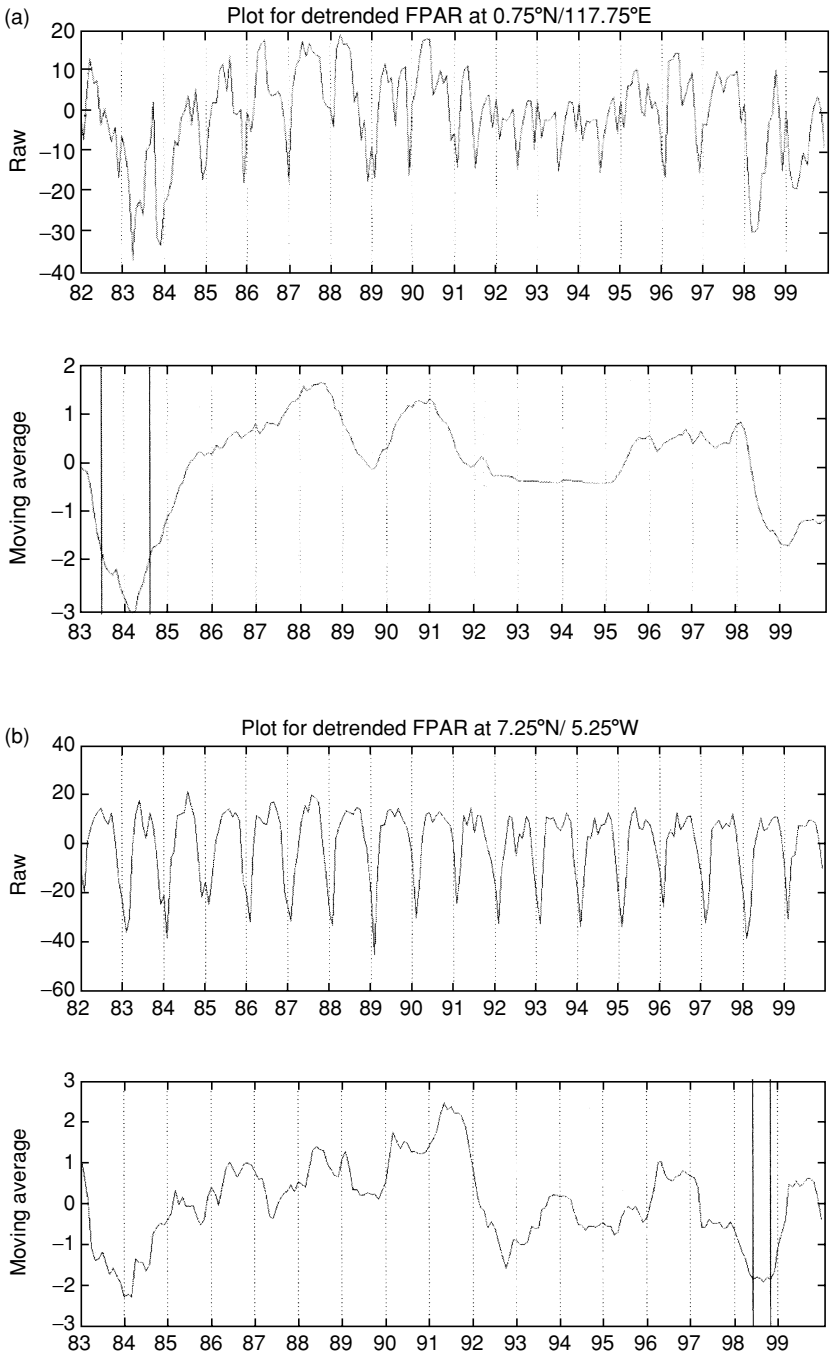

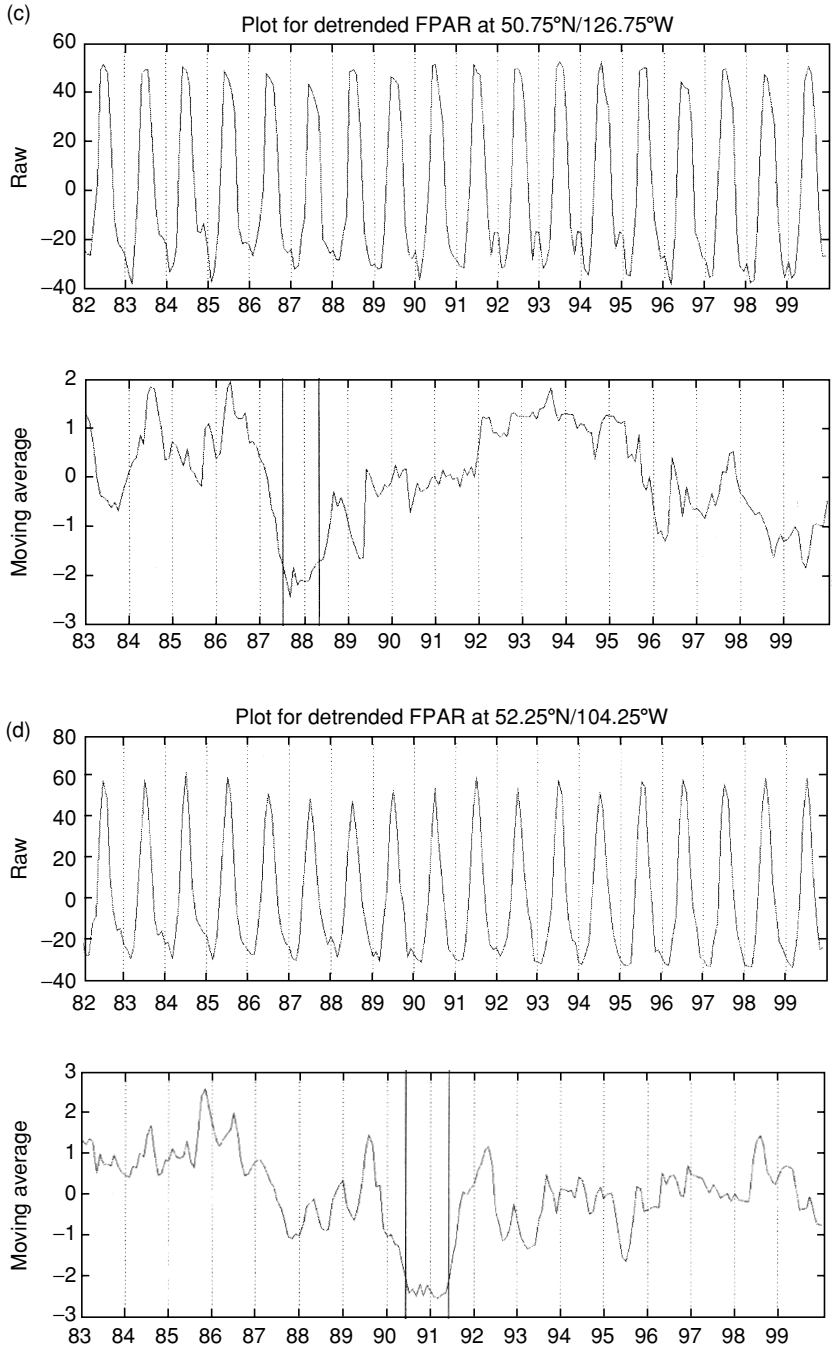
(c)
Plot for detrended FPAR at 50.75°N/126.75°W
Raw
Moving average
(d)
Plot for detrended FPAR at 52.25°N/104.25°W
Raw
Moving average

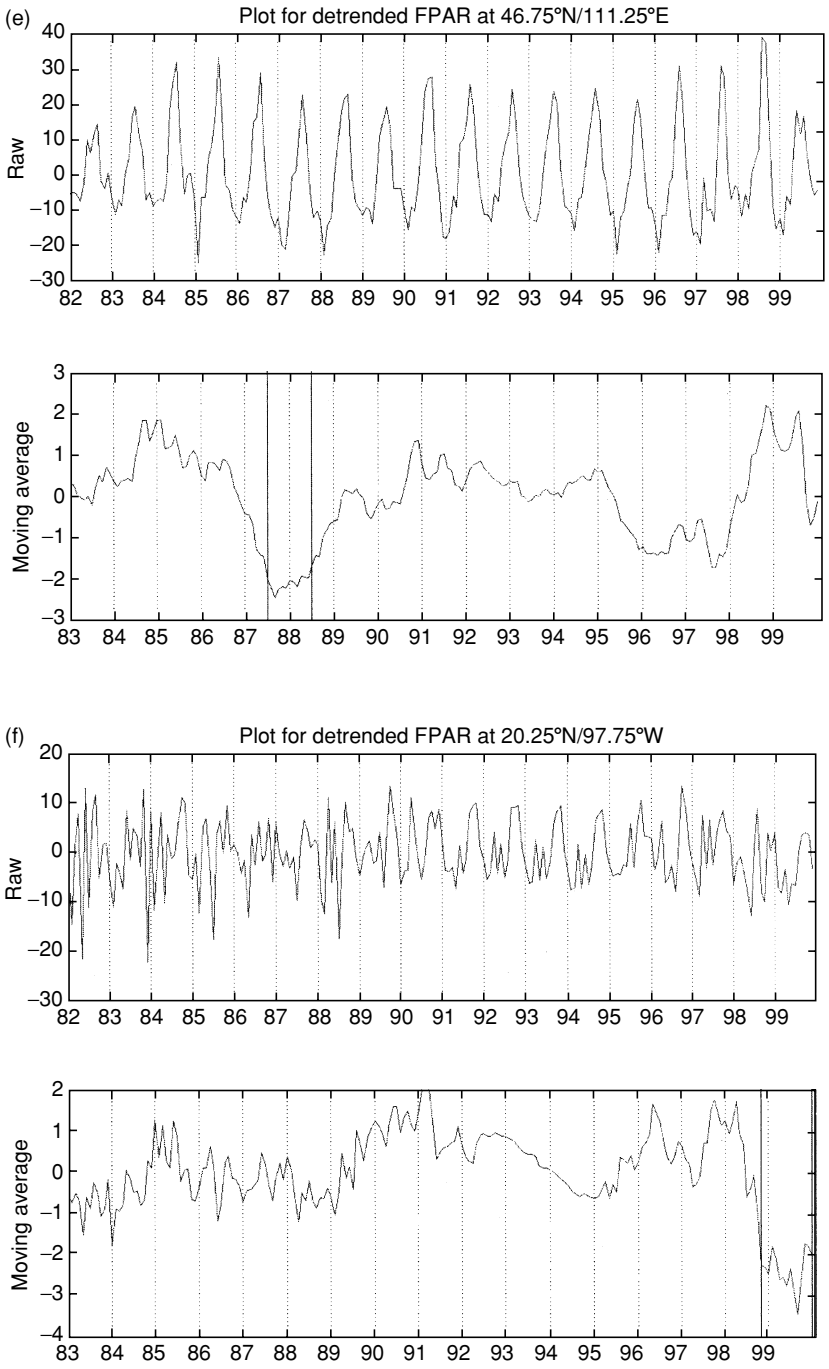

Fig. 6 Selected time series plots of detrended monthly FPAR values from 1982 to 1999; top panels are original (raw) FPAR values in units of percent, and bottom panels are the deseasonalized FPAR anomalies in units of SD in the 12 months moving average. Vertical lines show the longest consecutive period of anomalously LO monthly values. Owing to the use of a moving average, the apparent start time of the FPAR-LO events shown in the bottom panels may be up to 12-month shifted from the documented timing of wildfires reported in Table 2. (a) East Kalimantan and Indonesia, 1983, (b) Ivory Coast, 1983, (c) Russia–China, 1987, (d) Manitoba and Canada, 1989, (e) Mongolia, 1987, 1996, (f) Mexico, 1998.

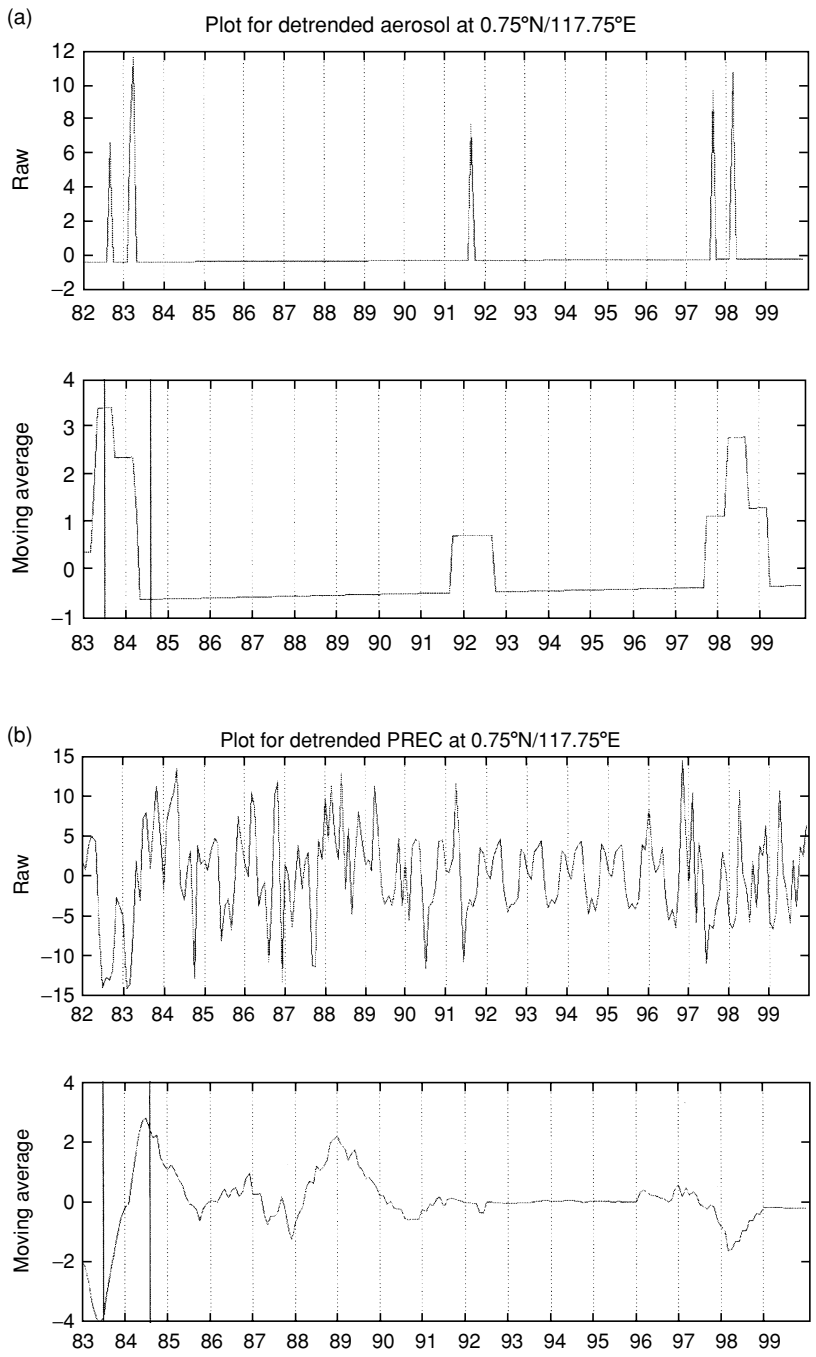

Fig. 7 (a) Smoke-aerosol index (SAI) and (b) monthly PREC for selected pixel location in East Kalimantan, Indonesia. The SAI is measured by the NASA Total Ozone Mapping Spectrometer (TOMS) instruments (Hsu *et al.*, 1996).

by the NASA Total Ozone Mapping Spectrometer (TOMS) instruments, from Nimbus-7 and Meteor-3 using measured 340 and 380 nm radiances, to ADEOS and Earth Probe TOMS using 331 and 360 nm wavelength channels (Hsu *et al.*, 1996). Daily global maps of the SAI at 1° resolution over land and water have been generated for much of the time series from 1982 to 1999. Some limitations of the SAI are that no absorbing aerosols can be detected close to the ground (below 1.5 km), and sensitivity is reduced under cloudy conditions. Nevertheless, for

all the selected disturbance event locations verified Fig. 6 (except the Manitoba Canada fires of 1989), elevated monthly values of the TOMS SAI could be detected during 1 or 2 months of the year documented for major wildfire events in Table 2.

It is important to note that not all the FPAR-LO events shown in Fig. 2 are necessarily wildfire-related. Our detection algorithm would locate any (other) major disturbance events, whether physical, biogenic, or anthropogenic in nature. For example, we can further verify the types of disturbance that were likely detected for the three main areas where the largest contiguous areas of potential disturbance (>2 Mha) may have occurred in the 18-year time series. For the northeastern portion of Brazil (centered 7°S/39°W) during 1983, Rao *et al*. (1997) have documented widespread crop failures throughout this region due to severe El Niño related drought. Likewise, for croplands in western India (centered 22°N/71°E) during 1986–1987, this pan-Asian drought was, in terms of temperature and precipitation anomalies, one of the worst of this century for the region of Gujarat, India (USAID, 2001). For northwestern Canada (centered 59°N/122°W) during 1995–1996, the British Columbia Ministry of Forests Annual Report cited numerous large forest fires in the areas around Fort Nelson and unprecedented fire-fighting activity in the region (Ministry of Forests and Lands, 1996).

In summary, our FPAR-LO method based on 0.5° AVHRR would without a doubt under-sample actual fire activity in biomes as complex as the global boreal forest or tropical savanna. The next logical step for this type of detection method would be to use higher resolution (maximum 1 km) AVHRR time series data to identify much smaller (<0.5 Mha each) fire-disturbed and burn scarred areas in these biomes with the same FPAR-LO method, and attempt to validate the results using spatially explicit satellite data sets for burned areas (Kasischke *et al*., 2002; Stocks *et al*., 2003)

Association with historical climate data

The FPAR record described in this study can be used to test the hypothesis that natural disturbance regimes are related to patterns of regional climate that can increase or decrease the probability of a major disturbance event. Hence, we made comparisons of the timing of major disturbance events shown in Fig. 2 with LO or anomalously high (HI) monthly records for surface air temperature (TEMP), precipitation (PREC), and solar irradiance (SOLAR) from 1982 to 1998 (Potter, 1999; New *et al*., 2000) that preceded FPAR-LO >12 months events, in order to reveal potential climate controls over disturbance regimes within major vegetation classes (DeFries & Townshend, 1994).

Anomalous climate events were identified by first converting the 18-year TEMP, PREC, and SOLAR records into Z-score time series by subtracting the monthly mean and dividing by the monthly standard deviation. Either HI or LO climate events were next defined whenever the monthly Z-score exceeded ± 1.7 SD, respectively. Climate events that preceded major disturbance events were identified as having occurred as HI or LO at least once within the 3-months time window just previous to the start month for any of the disturbance events shown at the pixel locations in Fig. 2b. We also included the first month of the >12 consecutive month FPAR-LO time series in the climate event set.

Results show the number of times (months), for anomalous climate events within the time window of 3 months prior to FPAR-LO disturbance events (Table 3). For example, the highest frequency was detected for the association of PREC-HI → FPAR-LO, which indicates that out of the 1173 total cases that an FPAR-LO >12 months event has occurred with at least one climate event within the 3 months window prior to the FPAR-LO event, 367 (31.3%) of these FPAR-LO events (31.3%) were preceded by at least one PREC-HI event. The majority of these PREC-HI → FPAR-LO associations occurred in savannas and wooded grassland ecosystems (57%) located mainly below 10°S latitude, and in boreal forest and tundra ecosystems (19%) located above 50°N latitude. The same distribution among ecosystem classes is represented in the association of SOLAR-LO → FPAR-LO, implying anomalously cloudy antecedent conditions. If PREC-HI and SOLAR-LO events have been commonly associated with high frequency of lightning strikes that ignite ground fires in these ecosystems, then this could explain the predominance of this association with FPAR-LO disturbance regimes globally. These results are consistent with the observation that fires set by lightning strikes account for 85% of the total forest area burned in Canada (Murphy *et al*., 2000; CIFFC, 2001).

Table 3 Frequency for the association of antecedent climate events with FPAR-LO events, as shown in Fig. 2

Antecedent climate event → FPAR-LO	Number of cases (%)
PREC-HI 'wet'	367 (31.3)
TEMP-LO 'cool'	262 (22.3)
PREC-LO 'dry'	244 (20.8)
SOLAR-LO 'cloudy'	243 (20.7)
TEMP-HI 'warm'	165 (14.1)
SOLAR-HI 'clear'	163 (13.9)
PREC-HI and TEMP-LO 'wet, cool'	86 (7.3)
PREC-HI and SOLAR-LO 'wet, cloudy'	77 (6.6)

Percentages do not total to 100 because anomalous climate events may occur in multiple combinations over a 3 months time period.

The next most common associations (with a frequency > 20% of the total) were detected for TEMP-LO → FPAR-LO and PREC-LO → FPAR-LO. More than 70% of the TEMP-LO → FPAR-LO associations occurred in savannas and grassland ecosystems mainly located in Africa and Australia. One explanation for this association could be given by the co-occurrence of TEMP-LO with PREC-HI antecedent conditions (Table 3). Nonetheless, this implication of cold temperature disturbance regimes requires further investigation for these ecosystems.

The majority of PREC-LO → FPAR-LO associations detected, which imply drought-related disturbance regimes, have occurred with almost equal frequency in savannas ecosystems (36%), and in boreal forest and tundra ecosystems (33%). A similar distribution among ecosystem classes is represented in the association of TEMP-HI → FPAR-LO, implying anomalously warm antecedent conditions in the disturbance regime.

Potential implications for the terrestrial carbon cycle

Fluxes of CO_2 from terrestrial biomass to the atmosphere during the major disturbance events identified in Fig. 2 can be computed using the NASA-CASA (Carnegie-Ames-Stanford) Biosphere model estimates of above-ground biomass (Potter, 1999; Potter *et al.*, 1999). NASA-CASA is a numerical model of monthly fluxes of water, carbon, and nitrogen in terrestrial ecosystems. Our estimates of terrestrial net primary production (NPP) fluxes depend on the same FPAR time series used to generate the disturbance maps in Fig. 2, together with the gridded climate from interpolated weather station records (New *et al.*, 2000). Our fundamental approach to estimating NPP is to define optimal metabolic rates for carbon fixation processes, and to adjust these rate values using scalars related to the limiting effects of SOLAR, TEMP, PREC, predicted soil moisture, and land cover (DeFries & Townshend, 1994). Carbon (CO_2) fixed by vegetation as NPP is estimated in the ecosystem model according to FPAR intercepted by plant canopies and a light utilization efficiency term (e_{max}). This product is modified by stress scalars for temperature (T_a) and moisture (W) that vary over time and space. The e_{max} term is set uniformly at 0.39 g C MJ^{-1} PAR (Potter *et al.*, 1993). Interannual NPP fluxes from the CASA model have been reported (Behrenfeld *et al.*, 2001) and validated against multiyear estimates of NPP from field stations and tree rings (Malmström *et al.*, 1997).

Global above-ground biomass is estimated in the NASA-CASA model as a function of residence times and allocation rates of carbon inputs from the predicted monthly NPP rates (Potter, 1999). Net primary production allocation among leaf, wood, and fine root tissues is defined as a set of fractional allocation constants of plant tissue pools (α) and the mean residence time (τ, in years) of carbon in the standing plant tissue pools. Soil fertility effects are included in this model version to adjust these allocation constants for generalized nutrient limitations. These above-ground biomass estimates from NASA-CASA have been verified on a regional basis (Houghton *et al.*, 2001).

We can begin to estimate biosphere-atmosphere fluxes with an assumption, perhaps conservative, that 50% of above-ground biomass carbon estimated by the NASA-CASA model (Potter, 1999) was eventually lost over the 18-year time period to the atmosphere at the same locations of major disturbance events shown in Fig. 2. The assumption of 50% biomass loss from major fire disturbance comes from studies of combustion efficiency of above-ground plant material monitored during biomass burning in tropical forest (Guild *et al.*, 1998; Sorrensen, 2000) and boreal forest (Kasischke *et al.*, 1995) ecosystems. In the case of other (nonfire) disturbance factors (drought, for example), we hypothesize that the disturbance processes detected as a significant FPAR-LO event have an equivalent effect (minimum 50% biomass loss as CO_2 to the atmosphere by organic matter decomposition) as does fire disturbance, but over seasonal time periods much longer than a major burning event.

At the hypothesized 50% loss level, the total for all vegetation types was nearly 9 Pg C over the entire 18-year time series (Table 4). The three vegetation classes contributing most strongly to this total carbon flux were savanna, broadleaf (tropical) evergreen forests, and boreal (coniferous) evergreen forests. The average annual flux of carbon to the atmosphere from major disturbance events would have been about 0.5 Pg

Table 4 Above-ground biomass carbon (estimated by the NASA-CASA model, Potter, 1999) lost over the 18-year time period to the atmosphere at the locations of major disturbance events shown in Fig. 2

	Predicted biomass C lost	
Vegetation classes (from Potter, 1999)	Total (Pg C)	Average (Pg C yr^{-1})
Broadleaf evergreen forest	1.29	0.07
Coniferous evergreen forest	1.43	0.08
High latitude deciduous forest	0.26	0.01
Tundra	0.17	0.01
Mixed coniferous–deciduous forest	0.35	0.02
Savanna and wooded grassland	2.98	0.17
Grassland	0.82	0.05
Desert	0.00	0.00
Cultivated	0.70	0.04
Broadleaf deciduous forest	0.30	0.02
Shrublands	0.46	0.03
Global total	8.77	0.49

C yr^{-1}. However, because the time series of disturbance area was observed as highly variable from year-to-year (Fig. 5), we hypothesize that 1.5 Pg C yr^{-1} could have been lost to the atmosphere from above-ground biomass carbon during the peak years of 1983 and 1996, with much lower fluxes in other years. This range of annual carbon losses from major disturbances in global terrestrial ecosystems closely matches the lower end of the range of annual flux rates estimated by Schimel *et al*. (2001) for global 'land use change' sources of carbon at between 0.6 and 2.5 Pg C yr^{-1} for the 1980s and 1990s.

Because relatively small-scale disturbance events such as slash and burn deforestation in tropical forests cannot be detected using satellite FPAR at 0.5° spatial resolution, a portion of the land use change source of carbon cannot be quantified in this time series analysis. Several other qualifications of these carbon flux predictions are necessary: (a) In savannas, grasslands, and cultivated areas, and many shrublands, some of the biomass that burns during a fire 1 year is recaptured rapidly through herbaceous plant growth during the following years of recovery. Thus, this carbon flux may not represent a net long-term loss to the atmosphere; (b) Our assumption that 50% of the above-ground biomass is consumed from burning of boreal forests may be an overestimate. If so, then the above-ground contribution of these forests may be over-predicted by about 20%; (c) Fires in boreal regions can consumed large amounts of organic matter present in the ground layer, e.g., organic soils (Kasischke *et al*., 1995). Hence, the full impact of fire on the atmospheric carbon budget in this region cannot be fully determined without consideration of this below-ground source of emissions.

Conclusions

A main objective of this study was to better understand historical global patterns of ecosystem disturbance events and to characterize major disturbance regimes in terms of spatial extent, geographical distribution, and frequency over time. To this end, we are able to draw several initial conclusions on the basis of results from analysis of the 18-year FPAR time series from AVHRR observations.

- *Vegetation classes with the highest frequency of major ecosystem disturbance are savannas, shrublands, and coniferous (boreal) forests.* Support for this conclusion comes from our study results (Table 1), and from analysis of the Global Fire Product (GFP) of the International Geosphere-Biosphere Programme, which provides a consistent data set on daily AVHRR satellite fire counts at the global scale (Stroppiana *et al*., 2000). Dwyer *et al*. (1998) reported that while fires could be detected in the GFP during 1992 for almost every region of the globe, the main vegetation types affected by fire were the savanna woodlands of the tropical zones. In regional analyses, Barbosa *et al*. (1999) found that about 70% of the total area burned in all of Africa for the period 1981–1991 were detected in savannas and wooded grassland zones. For Alaska and Canada, Murphy *et al*. (2000) reported that 98% of the total area burned for the period 1980–1994 was in the boreal forest zones.
- *There is high interannual variability in the global area of terrestrial ecosystem disturbance.* Support for this conclusion comes from our study results (Fig. 5), and from studies of fire disturbance regimes from Alaska to the southwestern United States, which indicate a history of forest fires dominated by large infrequent burns (Veblen *et al*., 1994). For example, there have been just two periods of major forest fire activity reported by the Canadian Forest Service since 1982, namely in 1989 and 1994–1995, when more than 6 Mha were burned (CIFFC, 2001). All other years were reported to have had less than 2 Mha forest area burned. During the past two decades, only 1.4% of forest fires in Canada exceeded 1000 ha in size, but these fires have accounted for 93% of the total area burned nationwide (Murphy *et al*., 2000). For Africa, Barbosa *et al*. (1999) reported a factor of two for interannual variability in area burned during the period 1981–1991.
- *The probability of major disturbance events increases with increased climatic variability.* Support for this conclusion comes from our study results (Table 3), and from North American tree-ring studies that show increases in areas burned are associated with years of above average precipitation, followed by springs and summers of below average precipitation (Veblen *et al*., 1994). Swetnam & Betancourt (1990) reported that large fires in the southwestern United States over three centuries were associated with deficient spring precipitation and reduced tree growth, which implies that seasonal climate patterns, and not just recent weather events, determine burning of vegetation on a subcontinental scale. Regional fires occur during extreme droughts, but antecedent wet conditions play an important secondary role by regulating accumulation of fuels. Based on analysis of extensive wildfires during 2000 in the western United States, Brown & Hall (2001) found that patterns of high wildfire activity were associated with a persistent climate pattern of below average precipitation, above average temperature, and below average relative humidity across large portions of the region, based on 40 years of climate records. At the same time, lightning occurrence was also wide spread throughout the season causing an above average number of natural fire starts.

Each of the conclusions presented above is subject to further verification using high spatial and temporal

resolution satellite data sources of land cover change in terrestrial ecosystems worldwide. We anticipate that a spatial resolution of several kilometers in global FPAR data sets will reveal many more interesting relations between climate and ecosystem disturbance over the past two decades.

Acknowledgements

This work was supported by grants from NASA programs in Intelligent Systems and Intelligent Data Understanding, and the NASA Earth Observing System (EOS) Interdisciplinary Science Program. The authors are grateful to C. Hlavka for thoughtful reviews of an earlier version of the paper.

References

Amiro BD, Todd JB, Wotton BM *et al.* (2001) Direct carbon emissions from Canadian forest fires, 1959–1999. *Canadian Journal of Forest Research*, **31**, 512–525.

Andreae MO (1991) Biomass burning: its history, use, and distribution and its impact on environmental quality and global climate. In: *Global Biomass Burning: Atmospheric, Climactic and Biospheric Implications* (ed. Levine JS), pp. 3–21. MIT Press, New York.

Arino O, Plummer S (1999) *Along Track Scanning Radiometer World Fire Atlas: Validation of the 1997–1998 Active Fire Product*. IGBP Report.

Barbosa PM, Grégoire J-M, Stroppiana D *et al.* (1999) An assessment of fire in Africa (1981–1991): burnt areas, burnt biomass and atmospheric emissions. *Global Biogeochemical Cycles*, **13**, 933–950.

Behrenfeld MJ, Randerson JT, McClain CR *et al.* (2001) Biospheric primary production during an ENSO transition. *Science*, **291**, 2594–2259.

Biasutti R, Marchetti M (1996) *Earth Watching from Eurimage – An 'Eye' on the World, A Near-real Time Monitoring Program for Floods, Fires and Oil Pollution.* Integrated Applications for Risk Assessment and Disaster Prevention for the Mediterranean, 20–23 May, Malta.

Boles SH, Verbyla DL (2000) Comparison of three AVHRR-based fire detection algorithms for interior Alaska. *Remote Sensing of Environment*, **72**, 1–16.

Brown TJ, Hall BL (2001) *Climate Analysis of the 2000 Fire Season, 2001*, Climate, Ecosystem and Fire Applications Program Report #01–02, 40 p. Reno, Nevada.

Cahoon DR Jr, Levine JS, Cofer WR III *et al.* (1991) The great Chinese fire of 1987: a view from space. In: *Global Biomass Burning: Atmospheric, Climatic, and Biospheric Implications* (ed. Levine JS). MIT Press, Cambridge, Mass.

Cahoon DR, Stocks BJ, Levine JS *et al.* (1994) Satellite analysis of the severe 1987 forest fires in northern China and southeastern Siberia. *Journal of Geophysical Research*, **99**, 18627–18638.

Canadell JG, Mooney HA, Baldocchi DD *et al.* (2000) Carbon metabolism of the terrestrial biosphere: a multi-technique approach for improving understanding. *Ecosystems*, **3**, 115–130.

Canadian Interagency Forest Fire Centre (CIFFC) (2001) *Canada Report 2001*. 6 p. Winnipeg, Canada.

DeFries R, Townshend J (1994) NDVI-derived land cover classification at global scales. *International Journal of Remote Sensing*, **15**, 3567–3586.

Dwyer E, Grégoire J-M, Malingreau JP (1998) A global analysis of vegetation fires using satellite images: spatial and temporal dynamics. *Ambio*, **27**, 175–181.

Fearnside PM (1997) Greenhouse gases from deforestation in Brazilian Amazonia: net committed emissions. *Climatic Change*, **35**, 321–360.

Galindo I, Lopez Perez P, Evangelista Salazar M (2003) Real-time AVHRR forest fire detection in Mexico (1998–2000). *International Journal of Remote Sensing*, **24**, 9–22.

Goldammer JG, Furyaev VV (1996) *Fire in Ecosystems of Boreal Eurasia*. 390 p. Kluwer Academic Publishers, Dordrecht, MA.

Guild LS, Kauffman JB, Ellingson LJ *et al.* (1998) Dynamics associated with total aboveground biomass, C, nutrient pools, and biomass burning of primary forest and pasture in Rondônia, Brazil during SCAR-B. *Journal of Geophysical Research*, **103**, 32091–32100.

Heinselman ML (1973) Fire in the virgin forests of the Boundary Waters Canoe Area, Minnesota. *Quaternary Research*, **3**, 329–382.

Hoffmann AA, Schindler L, Goldammer JG (1999) Aspects of a Fire Information System for East Kalimantan, Indonesia. In: *Proceedings of the Third International Symposium on Asian Tropical Forest Management, 20–23 September 1999.* Samarinda, East Kalimantan, Indonesia.

Houghton RA (1999) The annual net flux of carbon to the atmosphere from changes in land use 1850–1990. *Tellus*, **51B**, 298–313.

Houghton RA, Hackler JL (1999) Emissions of carbon from forestry and land-use change in tropical Asia. *Global Change Biology*, **5**, 481–492.

Houghton RA, Hackler JL, Lawrence KT (1999) The US carbon budget: contributions from land-use change. *Science*, **285**, 574–579.

Houghton RA, Lawrence KT, Hackler JL *et al.* (2001) The spatial distribution of forest biomass in the Brazilian Amazon, *Global Change Biology*, **7**, 731–746.

Hsu NC, Herman JR, Bhartia PK *et al.* (1996) Detection of biomass burning smoke from TOMS measurements. *Geophysical Research Letters*, **23**, 745–748.

Hurst DF, Griffith DWT, Cook GD (1994) Trace gas emissions from biomass burning in tropical Australian savannas. *Journal of Geophysical Research*, **99**, 16441–16456.

Jeffrey D (1989) Yellowstone: the great fires of 1988. *National Geography*, **175**, 255–273.

Kasischke ES, Bergen K, Fennimore R *et al.* (1999) Satellite imagery gives a clear picture of Russia's boreal forest fires. *EOS Transactions of the American Geophysical Union*, **80**, 141–147.

Kasischke ES, Christensen NL Jr, Stocks BJ (1995) Fire, Global warming and the mass balance of carbon in boreal forests. *Ecological Application*, **5**, 437–451.

Kasischke ES, French NHF, Bourgeau-Chavez LL (1999) Using satellite data to monitor fire-related processes in boreal forests. In: *Fire, Climate Change and Carbon Cycling in the Boreal Forest* (eds Kasischke ES, Stocks BJ), pp. 406–422. Ecological Studies Series, Springer, New York.

Kasischke ES, Williams D, Barry D (2002) Analysis of the patterns of large fires in the boreal forest region of Alaska. *International Journal of Wildland Fire*, **11**, 131–144.

Kaufman YJ, Hobbs PV, Kirchhoff VWJH *et al.* (1998) Smoke, clouds, and radiation-Brazil (SCAR-B) experiment. *Journal of Geophysical Research*, **103**, 31783–31808.

Knyazikhin Y, Martonchik JV, Myneni RB *et al.* (1998) Synergistic algorithm for estimating vegetation canopy leaf area index and fraction of absorbed photosynthetically active radiation from MODIS and MISR data. *Journal of Geophysical Research*, **103**, 32257–32276.

Kurz WA, Apps MJ (1999) A 70-years retrospective analysis of carbon fluxes in the Canadian forest sector. *Ecological Applications*, **9**, 526–547.

Malmström CM, Thompson MV, Juday GP *et al.* (1997) Interannual variation in global scale net primary production: testing model estimates. *Global Biogeochemical Cycles*, **11**, 367–392.

Ministry of Forests and Lands (1996) *Annual report of the Ministry of Forests and Lands*, 98 p. Victoria, British Columbia.

Murphy PJ, Mudd JP, Stocks BJ *et al.* (2000) Historical fire records in the North American boreal forest. In: *Fire, Climate Change, and Carbon Cycling in the Boreal Forests*, Chap. 15 (eds Kasischke ES, Stocks BJ), Springer. New York.

Myneni RB, Tucker CJ, Asrar G *et al.* (1998) Interannual variations in satellite-sensed vegetation index data from 1981 to 1991. *Journal of Geophysical Research*, **103**, 6145–6160.

Nepstad DC, Veríssimo A, Alencar A *et al.* (1999) Large-scale impoverishment of Amazonian forests by logging and fire. *Nature*, **398**, 505–508.

New M, Hulme M, Jones P (2000) Representing twentieth century space-time climate variability. II. Development of 1901–1996 monthly grids of terrestrial surface climate. *Journal of Climate*, **13**, 2217–2238.

Pickett STA, White PS (1985) *The Ecology of Natural Disturbance as Patch Dynamics*. Academic Press, New York.

Potter CS (1999) Terrestrial biomass and the effects of deforestation on the global carbon cycle. *Bioscience*, **49**, 769–778.

Potter CS, Brooks-Genovese V, Klooster SA *et al.* (2001) Biomass burning losses of carbon estimated from ecosystem modeling and satellite data analysis for the Brazilian Amazon region. *Atmospheric Environment*, **35**, 1773–1781.

Potter CS, Klooster SA, Brooks V (1999) Interannual variability in terrestrial net primary production: exploration of trends and controls on regional to global scales. *Ecosystems*, **2**, 36–48.

Potter CS, Randerson JT, Field CB *et al.* (1993) Terrestrial ecosystem production: a process model based on global satellite and surface data. *Global Biogeochemical Cycles*, **7**, 811–841.

Rao VB, Sa LDA, Franchito SH *et al.* (1997) Interannual variations of rainfall and corn yields in northeast Brazil. *Agriculture Forest Meteorology*, **85**, 63–74.

Schimel D, House J, Hibbard K *et al.* (2001) Recent patterns and mechanisms of carbon exchange by terrestrial ecosystems. *Nature*, **414**, 169–172.

Scholes RJ, Kendall J, Justice CO (1996) The quantity of biomass burned in southern Africa. *Journal of Geophysical Research*, **101**, 23667–23676.

Shovic H (1988) *Preliminary Burned Area Survey of Yellowstone National Park and Adjoining National Forests, Project Summary and Tabular Areas, December 1998.* National Park Service and US Forest Service, Yellowstone, Wyo.

Sorrensen CL (2000) Linking smallholder land use and fire activity: examining biomass burning in the Brazilian Lower Amazon. *Forest Ecology Management*, **128**, 11–25.

Stockburger DW (1998) Introductory statistics: concepts, models, and applications, WWW Version 1.0. [http://www.psychstat.smsu.edu/sbk00.htm].

Stocks BJ, Mason JA, Todd JB *et al.* (2003) Large forest fires in Canada, 1959–1997. *Journal of Geophysical Research*, **108**, 5-1–5-12.

Stroppiana D, Pinnock S, Grégoire J-M (2000) The global fire product: daily fire occurrence from April 1992 to December 1993 derived from NOAA-AVHRR data. *International Journal of Remote Sensing*, **21**, 1279–1288.

Swetnam TW (1996) Fire and climate history in the Central Yenisey Region, Siberia. In: *Fire in Ecosystems of Boreal Eurasia* (eds Goldammer JG, Furyaev VV), pp. 90–104. Kluwer, Dordrecht.

Swetnam TW, Betancourt JL (1990) Fire-southern oscillation relations in the southwestern United States. *Science*, **249**, 1017–1021.

Tilman D (1985) The resource-ratio hypothesis of plant succession. *American Naturalist*, **125**, 827–852.

US Agency for International Development (USAID) (2001) *India – Drought Fact Sheet #1*, Washington, DC.

Veblen TT, Hadley KS, Nel EM *et al.* (1994) Disturbance regime and disturbance interactions in a Rocky Mountain subalpine forest. *Journal of Ecology*, **82**, 125–135.